INITIAL STATE SENSITIVITY EXPERIMENTS IN A REAL DATA MODEL

Celeste A. Saulo (1), Lee A. Byerle*(2), Jennifer C. Roman (2),
Jan Paegle (2) and Julia Nogués-Paegle (2)

(1) University of Buenos Aires, Argentina
(2)University of Utah, Salt Lake City, Utah

1. INTRODUCTION

The present research suggests the feasibility of global, real-time prediction in small research groups that have access to gridded operational analyses in near-real time. Real-time global weather prediction with the Utah Global model (UGM) has been performed with research models at the University of Utah since summer 2002. These forecasts have been compared with operational forecasts from NCEP (e.g., Roman et al., 2004). As expected, the operational models provide substantially higher accuracy for two-week prediction. Nevertheless, the error patterns in research and operational models are often remarkably similar (Roman et al., 2004).

Additionally, the real-time UGM integrations provide the opportunity to examine atmospheric processes anywhere on the globe within a day or so of receiving the global grids from NCEP. This provides a useful diagnostic and forecast tool for case studies and/or to complement field programs. An example of this is over subtropical South America during the summer season, which has recently been the venue of an international field program to observe low-level jets (LLJs) east of the Andes.

The observing system over Central and South America has recently been improved by addition of several pibal soundings from PACS-SONET (http://www.nssl.noaa.gov/projects/pacs). In addition, the South American Low-Level Jet Experiment (SALLJEX) was recently conducted to observe low-level circulations east of the Andes (http://www.clivar.org/organization/vamos/index.htm). The goal of this paper is to present preliminary predictability studies with the UGM that are designed to anticipate the sensitivity of weather prediction in the South American region to atmospheric detail that is included or excluded in the specification of the initial state over and around South America.

The SALLJEX data were undergoing quality control at the start of this project, and inclusion in the UGM still requires completion of the assimilation effort. The data sets used to initialized the model here are operational NCEP Global Data Assimilation System (GDAS) analyses as well as NCEP/NCAR Reanalyses (Kalnay et al., 1996; and Kistler et al., 2001).

2. MOTIVATION FOR EXPERIMENTS

Prediction of weather and short range climate evolution over South America is characterized by different challenges than those that arise for North America. This study focusses upon special challenges posed by observation gaps in the Southern Hemisphere (SH) atmosphere. The operational observing network of land radiosondes is much more sparse here (e.g., see Fig. 1 of Saulo et al., 2001) than over the Northern Hemisphere (NH), while the southern oceans may be observed almost as well by satellites as are the northern oceans. It is consequently unclear whether data sparse regions of the oceans or continents represent

**Corresponding author address*: Lee Byerle, Univ. of Utah Dept. of Meteorology, Salt Lake City, UT 84112; e-mail: labyerle@met.utah.edu.

the most strongly limiting components of the southern observing system. The relative importance of initial state detail over South America and detail external to South America is examined with a set of experiments using the variable resolution UGM designed to assess impact of initial state changes upon regional predictability.

Several studies have focussed upon the impact of supplemental observations within data sparse regions of the western hemisphere upon forecasts over populated regions of North America. Langland et al. (1999) evaluated the role of experimental dropsonde data over the north Pacific upon short range weather prediction over North America. The additional data collected during the North Pacific Experiment (NORPEX) in January and February 1998 were included within the data assimilation system of the Medium Range Forecast (MRF) model. A phase of the California Land-Falling Jets Experiment (CALJET) also took place during the same winter (Ralph et al., 1999). This latter experiment was designed to obtain observations for improved forecast guidance in the 0-12 hour range. Both CALJET and NORPEX field experiments have been repeated during more recent winters. Other field projects designed to improve understanding and forecasting of winter weather events over the complex geography of western North America include the Intermountain Precipitation Experiment (IPEX, Schultz et al., 2002) and Improvement of Microphysical Parameterization through Observational Verification Experiment (IMPROVE, Stoelinga et al., 2003).

The added observations obtained in experiments such as NORPEX show a positive impact upon short term forecasts over North America. The improvement is particularly evident over western portions of the U.S. in which the forecast skill of a variety of operational and research models has been shown to be remarkably similar by White et al. (1999). White et al. (1999) suggest that the proximity of the data sparse region of the Pacific has negative impact upon both highly resolved and well developed models, as well as less sophisticated models, and that this may be the main limitation to accurate winter weather prediction at 36 hours over the western U.S.

The NORPEX dropsondes were deployed over the north Pacific instead of North America because the North American region is relatively well analyzed by the high density, operational radiosonde stations. Much of North America is situated in the zone of ambient westerly winds within which weather events propagate rapidly from west to east, particularly during the winter season. Atmospheric changes tend to move eastward quickly from the north Pacific across North America on a time scale of approximately 5 days or less during the northern winter (Langland et al., 1999; and Miguez-Macho and Paegle, 2001).

By contrast, the characteristics of the South American observing system and regional weather evolution are rather different. Much of South America is located in the tropics and subtropics within which eastward propagation of Rossby wave influences is relatively slow, particularly during the important warm seasons that tend to be wet over the continent.

Several field programs have been mounted over South America with the intent to improve atmospheric observations here. Some projects, such as the Atmospheric Boundary Layer Experiment (ABLE 2B, Garstang et al., 1990), have studied surface processes over the Amazon basin, with particular emphasis on evapotranspiration. Nicolini et al. (2002) show that better surface observations and treatment of surface conditions are more important than improved specification of initial state uncertainty for short range, limited area predictions over South America. Limited area model sensitivity to initial condition uncertainty is, however, diminished by use of boundary conditions that constrain error growth (e.g., Anthes, 1983; and Errico and Baumhefner, 1987). Uncertainty of lateral boundary conditions has been found to be more important than

initial state uncertainty in some regional model simulations (e.g., Paegle et al., 1997). Nicolini et al. (2002) demonstrate a similarly important role for the specification of the bottom boundary condition.

Global models are required to minimize the overwhelming role of lateral boundary constraints upon error growth of limited area models. Unfortunately, global models often have relatively coarse resolution, and this limits their local utility in regions such as South America, where the Andes mountains impose first order influences upon regional weather evolution (e.g., Kleeman, 1989; Gandu and Geisler, 1991; and Campetella and Vera, 2002). The Andes present a special challenge to numerical simulation because of their effective ridge heights extending to the midtroposphere and mesoscale east-west dimensions.

The purpose of this research is to address the question of initial state uncertainty growth over South America. A variable resolution version of the global model described by Paegle (1989) is used, and except for variable resolution it is very similar to the one used by Miguez-Macho and Paegle (2001, hereafter, MMP01) for NH inital state modifications.

The approach is to initialize the UGM first with the coarse resolution NCEP/NCAR Reanalyses globally in a control integration. Experimental integrations are then performed in which the reanalyses are replaced with higher resolution, NCEP Global Data Assimilation System (GDAS) analyses. The GDAS analyses are intended to serve as proxies for analyses including higher resolution observations. The switch from Reanalysis to GDAS initial states is performed globally and over South America to study the potential predictability impact of initial state changes in different portions of the globe.

Section 3 describes the global analyses; the rotated, variable resolution UGM; and the methodology for data changes over selected regions. MMP01 examined the sensitivity of initial state data changes on medium range forecasts over North America during winter using a uniform resolution version of the UGM. Section 4 repeats similar experiments for northern winter 2003, using the rotated, variable resolution UGM, more suited for South America. The results and conclusions for midlatitudes of northern winter are similar to MMP01 and are included for comparison to the South American data sensitivity tests, presented in Section 5. Section 5 also presents numerical tests of the suitability of the rotated, variable resolution approach. Section 6 provides further discussion and section 7 a summary.

3. DATA, MODEL AND EXPERIMENT DESIGN

3.1 Datasets

The NCEP/NCAR Reanalysis is a state-of-the-art, retrospective analysis of assimilated observations which uses a frozen data assimilation system (Kalnay et al., 1996). The horizontal resolution is 2.5˚ with wave number 37 truncation, and there are 26 vertical levels. Operational GDAS analyses are used to initialize NCEP's Global Forecast System (GFS) model at wave number T254. GDAS data have horizontal resolution of 1˚ on 26 vertical levels and are available via anonymous file transfer protocol (ftp.prd.ncep.noaa.gov).

Fig. 1 presents magnitudes of 500 mb wind differences between the Reanalysis and GDAS on 17 January 2003, 00 UTC. Differences are generally on the order of 5 m/s. They tend to be largest over the oceans (maximum 18 m/s), near the poles and over data sparse land regions, where lack of conventional surface based rawinsonde data may produce values that are strongly influenced by the forecast model used for the first guess.

Notable differences are also evident over the southeastern U.S. (about 15 m/s) and off the western coast of Ireland.

The enstrophy spectrum of the two global analyses is examined next. Enstrophy is the square of the vorticity field, and its spectrum emphasizes shorter waves. The streamfunction is first computed globally from the wind field, and then projected onto spherical harmonics. Globally integrated enstrophy may be expressed as:

$$\int_A (\nabla^2 \Psi)^2 \, DA = \sum_{mn} \left(A_n^m \right)^2 [n(n+1)]^2 \qquad (1)$$

where A is the global area, Ψ is streamfunction; and A_n^m is the amplitude coefficient of the spherical harmonic component of degree *n* and order *m*. The quantity:

$$\left[\sum_m \left(A_n^m \right)^2 \right]^{\frac{1}{2}} \qquad (2)$$

is plotted against global wave number *n* in Fig. 2, for 30 January 2003 at sigma level 0.2. The highest values are evident in the lowest wave numbers. The GDAS analysis contains higher enstrophy in the larger wave numbers, while the Reanalysis spectrum drops abruptly beyond wave number 30 (Fig. 2).

3.2 Rotated, Variable Resolution Model

The UGM was originally developed by Paegle (1989) with a variable resolution capability designed to address predictability questions of the sort particularly relevant in the present application. A variable resolution version of the model has been used in barotropic predictability experiments by Paegle et al. (1997). The primitive equation version of the rotated, variable resolution version is presented here. More details of the UGM are described in Paegle (1989); and Roman et al. (2004).

Fig. 3 demonstrates the uniform and rotated, variable resolution model grid and topography. The method takes advantage of the convergence of the meridians and therefore closer spacing between grid points near the polar regions (Fig. 3a). The mathematical north pole is shifted to 10˚S, 60˚W, in Fig. 3b. Higher resolution near the rotated north pole and surrounding region is obtained by increasing the concentration of latitudinal grid points north of 45˚N while decreasing the resolution to the south with respect to the mathematical grid (Fig. 3b). The configuration is similar to 2-way nested grid techniques available in other models in which resolution changes abruptly. For example, Cote et al. (1998a,b) employ a rotated, variable resolution model for application to a broad range of time scales. Unlike the method applied here, the mathematical poles are rotated away from the high resolution inner domain.

In Fig. 3b, equally spaced, 3˚ latitude increments extend from from the south pole, northward to 44˚N. Latitudinal spacing decreases to 1˚ from 45˚N to the mathematical north pole, situated at 10˚S, 60˚W. There are 91 grid points in latitude, 128 in longitude and 23 levels in the vertical. Experiments with the 2-way nested grid targeting South America are initialized at 00 UTC, 17 January 2003 and 12 UTC, 30 January 2003. Results of the former initialization time are described in section 5.

For comparison to the experiments which focus upon South America, results which target the NH during winter (section 4) are presented first. These contrast with experiments done previously at uniform resolution with

the UGM by MMP01. Here, the same version of the UGM is employed, with the mathematical north pole centered over the northeast Pacific Ocean (31˚N, 152˚W). The simulations are initialized at 12 UTC, 2 February 2003.

The time step is 400 seconds. Surface latent heat flux is specified over the globe using the 49 year, NCEP/NCAR Reanalysis monthly average corresponding to the month the integrations are initialized (January or February). Graphical representation of model output requires interpolation to a uniform, 1˚ resolution global grid.

3.3 Experiment Design

The approach is to first initialize the model with coarse resolution analyses in a control integration, and to subsequently replace these coarse analyses with higher resolution analyses. The higher resolution initial state transplants are performed globally, and in separate experiments that target the South American (northeast Pacific) sector as well as all regions outside South America (outside the northeast Pacific). The switch from Reanalysis to GDAS initial states is performed in selected regions to study the potential predictability impact of initial state changes in different portions of the globe, including some that correspond to the South American sector within which analyses may be influenced by the SALLJEX and PACS-SONET observations. Results are compared to similar experiments conducted over the NH during winter (e.g., MMP01). This new work uses the variable resolution approach and higher resolution GDAS initial data, allowing more sensitivity to initial state refinements than was found by MMP01.

4. INITIAL DATA CHANGES OVER NORTHEAST PACIFIC

The initial conditions of the control experiment (from the NCEP Reanalysis) are perturbed by changing them to GDAS analyses over a zone of the northeast Pacific that extends in a 20˚ latitudinal radius around the mathematical north pole (31˚N, 152˚W). The change from Reanalysis to GDAS is done smoothly with 5 grid points of linear transition from 66˚N to 71˚N of the mathematical grid. The region extends from approximately 10˚N to just south of the Aleutian Island chain (51˚N); and from near the dateline to the western coast of North America (Fig. 4). The initial time is 17 February 2003 at 12 UTC.

A complementary experiment is also performed where the change in initial state analysis is made over the rest of the globe and external to the northeast Pacific Ocean. The validation domain is in the region of the box in Fig. 4.

Fig. 4 portrays the meridional wind differences at sigma level 0.525 between the experiment initialized with the NCEP Reanalysis globally and the GDAS analysis over the northeast Pacific. At the initial time (Fig. 4a), differences between the Reanalysis and GDAS are only apparent over the northeast Pacific and gradually diminish to zero over the transition zone. Differences peak at about 10 m/s. After 96 hours, differences are found mainly outside of the domain and eastward, and peak values have decreased (Fig. 4b).

Fig. 5 displays the differences in the midtroposphere meridional flow between the experiments initialized with the Reanalysis and GDAS globally. Initial differences (Fig. 5a) are highest over the Rocky Mountains (near 15 m/s) and in the Gulf of Alaska (near 12 m/s). Differences after 96 hours have similar magnitudes (Fig. 5b).

The next experiment uses the NCEP

Reanalysis within the northeast Pacific region and the GDAS analysis outside this zone for the initial state. Differences in meridional flow at sigma 0.525, relative to the control (NCEP Reanalysis), are presented in Fig. 6. At the initial time (Fig. 6a) differences are zero over the northeast Pacific. Differences at 96 hours (Fig. 6b) look very similar to the pattern of Fig. 5b, which shows the differences in the forecast when the initial data change is made globally.

The initial, regional data change over the northeast Pacific (Fig. 4a) represents a small contribution to the total, global forecast differences after 96 hours (compare Fig. 4b and Fig. 5b). The complementary experiment represents a larger contribution to global forecast differences after 96 hours (Fig. 6b). Results therefore support the similar conclusion of MMP01: that the initial state modifications made over the northeast Pacific are not as important as initial state differences external to the region at 96 hours, even in the new rotated, variable resolution case using GDAS analyses.

The forecasts of the experiments relative to the control are quantified with variances computed over the northeast Pacific validation domain:

$$\text{variance} = \frac{\int_A (v_s - v_{con})^2 DA}{\int_A DA}, \qquad (3)$$

where A is the area of the validation (northeast Pacific region; e.g., box in Fig. 4a), v_s is the meridional wind component for the considered experiment and v_{con} for the control, which uses initial data globally from the NCEP/NCAR Reanalysis.

Fig. 7 shows variances at sigma 0.525 of the meridional wind. The solid curve is for the experiment with the global initial data change. It exhibits no growth through about the first 3 days of the forecast. The dotted curve with solid circles represents the experiment with the initial data change over the northeast Pacific. The variance is equal to that of the global difference experiment at the initial time, and it subsequently decreases to near 0 after 60 hours.

The variance of the meridional flow for the experiment with initial uncertainty outside the northeast Pacific is given by the dotted curve with open circles (Fig. 7). It is 0 at the initial time, and increases to equal the effect of the regional data change experiment after about 24 hours. It gradually increases after 48 hours and evolves similarly to the experiment with initial data changes made globally. Similar diagnostics are now applied for the experiments which target South America.

5. INITIAL DATA CHANGES OVER SOUTH AMERICA

Fig. 8 shows meridional wind differences for the regional targeting experiment where the data is switched from the Reanalysis to GDAS over South America. The mathematical pole of the UGM has been rotated to southwestern Brazil for these experiments (10˚S, 60˚W). Differences in the low-level meridional flow (sigma 0.875) are also presented (Fig. 8b). Initial differences peak at about 7 m/s at both atmospheric levels around South America, and they become zero outside of the transition zone. After 96 hours, maximum differences are near 9 m/s and are situated mainly within the targeted region of South America (Fig. 8c and d). Forecast differences to the southeast of South America continue evolving downstream in the subtropics beyond 4 days (not

shown).

Fig. 9 displays the differences in the midtroposphere and low-level meridional flow between the experiments initialized on 17 January with the Reanalysis and GDAS globally (Reanalysis minus GDAS). At forecast hour 96, differences are near 17 m/s in some midlatitude locations in both the mid and lower troposphere (Fig. 9c and d). The magnitudes of the differences over South America are generally comparable to those at the initial time, with the exception of the Andes region in the lower troposphere (Fig. 9d).

Complementary experiments to those which target uncertainty over South America are displayed in Fig. 10. The initial data change between the Reanalysis and GDAS is made outside of the South American region. The forecast difference with respect to the control is therefore zero over the South American region. Initial differences are largest near 40˚S over South America (Fig. 10a and b), in the vicinity of troughs analyzed in the mid and lower troposphere by the Reanalysis (not shown). After 96 hours, peak forecast differences are in the midlatitudes (Fig. 10c and d). Compared to the winter cases of section 4, the experiments with initial uncertainty inside and outside of South America (Fig. 8c and Fig. 10c, respectively) both produce similar response magnitudes as does the experiment in which initial uncertainty is prescribed globally (Fig. 9c). In the lower troposphere of the simulation with uncertainty outside of South America (Fig. 10d), the contributions to the global, meridional wind differences (Fig. 9d) are somewhat smaller, locally, compared to forecast differences for the experiment with initial uncertainty targeting South America (Fig. 8d). Results suggest that initial, local data changes over South America may affect the lower troposphere forecast evolution for a longer time when compared to targeted winter cases of the NH (section 4).

Forecast differences are quantified in Fig. 11 as in section 4 (see equation 3) with variances computed over the South American region (e.g., box in Fig. 8a). Fig. 11a shows the variance in the meridional wind at sigma 0.525. The solid line represents the difference between experiments initialized globally with the Reanalysis and GDAS. The variance increases steadily through most of the forecast. The experiment in which the switch from Reanalysis to GDAS is done over South America (solid circles) has similar magnitude as the global data change experiment at hour 0 and steadily decreases through the first 36 hours. Variance for the experiment in which that data is changed from Reanalysis to GDAS externally to South America is depicted as open circles. The curves for the two latter experiments (solid circles and open circles) evolve similarly in the midtroposphere from about day 1 to day 3.5 (Fig. 11a).

Results for the lower troposphere meridional wind and specific humidity variance are plotted in Figs. 11b and c. Initial state changes made locally (solid circles) contribute at least as much as or more to the total variance through the first 4 to 4.5 days of prediction as in the case where initial data changes occur outside of South America (open circles) (Fig. 11b). The impact of the local specification on moisture predicted at sigma level 0.875 is also evident through the first 4 days of prediction (Fig. 11c).

Curves containing boxes represent the variance evolution for additional experiments which examine the impact of numerical irregularities that may arise in the rotated, variable resolution approach. The “control” run for these experiments is the same configuration as in all previously described experiments except it uses the GDAS analysis globally instead of the NCEP Reanalysis.

The curve labelled “GDAS MR” (solid boxes, Fig. 11) is for an experiment initialized with GDAS analyses over the globe, and

the north pole is located over southwest Brazil (as in all previous runs); but it has higher resolution in latitude, using 141 points (as opposed to 91 in the control). Therefore, the higher resolution (1˚) inner nest covers a larger region (1 hemisphere), and the perimeter of the 2-way nest is more distant from the region of concern. The resolution is 1.8˚ outside of this hemispheric cup. Forecast differences between this experiment and the control quantify the impact of the abrupt resolution change in latitude which occurs in the control run. The transition in the control is from a 1˚, inner nest, to a 3˚, outer global region, taking place at 45˚ of the mathematical pole. As in previous experiments, the output for each simulation is interpolated to a uniform, 1˚ global grid to examine the differences. Evolution of the "GDAS MR" curve for each of the variables in Fig. 11 suggests that the impact of the abrupt transition zone is minimal relative to impacts in the other experiments.

The curve labelled "GDAS HI" (open boxes, Fig. 11) is an experiment in which the configuration in latitude is that same as "GDAS MR," but the resolution in longitude is also increased to 257 equally spaced points, corresponding to 1.4˚ longitude resolution. A measure of the variance in this experiment with respect to the same control as "GDAS MR" (GDAS globally) provides a further measure of the impact of the abrupt transition zone in latitude of the control. As with "GDAS MR," the variance is small relative to that in other experiments. The variance increases in both the mid and lower troposphere beyond day 4 of the forecast (Fig. 11a-c), but it remains below the sensitivity of the other experiments through day 7. It is concluded that numerical methods associated with the rotated pole, variable resolution approach do not produce notable distortion, and that results do not change strongly with resolution enhancement.

6. DISCUSSION

Saulo et al. (2001) show relatively slow growth of forecast errors over South America. In some instances and locations, short term forecast errors of the MRF were found by Saulo et al. (2001) to be smaller than analysis errors. One possible interpretation of this result is that the initial state errors here are so large that they are not substantially exceeded by forecast errors in short term predictions. Another possibility is that other components of the forecast problem, i. e., especially complex orography, a rainforest with poorly specified land use properties, and tropical convection, are of overwhelming importance. Finally, lateral boundary conditions may have constrained the sensitivity of those experiments. Related uncertainties may strongly constrain predictability even with accurate specification of the atmospheric state. This chapter presents results of preliminary experiments which examine the importance of initial state detail over and around the region during summer in a global model. During the summer wet season, the lower troposphere has particular significance through its role in water vapor transport, such as the moisture corridor the east Andes LLJ provides between the Amazon and La Plata region.

The 17 January experiments suggest that forecasts of lower troposphere winds are strongly influenced by detail of the initial state specification over South America through about the first 4-5 days of prediction. On the other hand, marked sensitivity of uncertainty impact is found for different synoptic situations used for the initialization, such as the case initialized on 30 January (not shown). Experiments for 30 January contain less variance in moisture and low-level wind over South America, and the influence of local targeting relative to external targeting is about the same from about day 2-4 (not shown).

The small case sampling does not suffice to systematically quantify the importance of initial conditions over the SALLJEX region. They do suggest that initial information over South America may be at least as important as initial state specification outside the region in some events (section 5), and this was never the case in MMP01. The latter study constitutes 34 different NH, midlatitude, winter cases. Preliminary results of this chapter imply an important role for in-situ observations for both the description and prediction of the regional and continental-scale hydrologic cycle over South America.

Tests for numerical irregularities associated with the rotated, variable resolution UGM have not been previously documented. Variance evolution of various model configurations has been used to quantify the impacts for the cases targeting South America. Results suggest the feasibility of the present rotated, 2-way nest approach for these time scales, and support the utility of the method in present applications. Similar tests examining a rotated, global variable resolution setup have been documented by Cote et al. (1998b). Their method rotates the mathematical poles away from the inner nest, producing a more isotropic subregion. They find "acceptably small" differences between rotated and uniform simulations over and around the inner domain at the 48 hour point (see their Fig. 7). UGM results also suggest that the chosen modeling technique is not as important as the seasonality or data sparsity over the targeted regions. Repeating the experiments of MMP01 over northern midlatitudes during winter with the rotated approach yields similar results to the earlier, unrotated experiments (section 4).

7. SUMMARY

This study assesses the impact of initial state changes upon regional predictability over South America using real-time gridded analyses and a global research model. It is unclear whether data sparse regions of the oceans or continents represent the most strongly limiting components of the southern observing system. The relative importance of summer initial state detail over South America and detail external to South America are studied with a set of experiments using a rotated, variable resolution version of the UGM. GDAS analyses represent surrogates for analyses which include higher resolution observations. Results are compared to similar experiments which target NH midlatitudes during winter.

In the latter experiments, initial, regional data changes over the northeast Pacific represent a small contribution to the total, global forecast differences after 4 days. Results support the conclusion of Miguez-Macho and Paegle (2001, MMP01) that initial state modifications made over that region during winter are not as important as initial state differences external to the northeast Pacific through 96 hours into the forecast. This result is also found using the new rotated, variable resolution approach and higher resolution GDAS analyses.

Over South America, targeting experiments are initialized on 17 and 30 January 2003, and results of the former are detailed here. Forecasts of lower troposphere winds and moisture are strongly influenced by detail of the initial state specification over South America through about the first 4-5 days of prediction. Therefore, initial information over South America may be at least as important as initial state specification outside the region in some summer events. This was never the case after 36 hours for MMP01, whose investigation included 34 different NH, midlatitude, winter cases. Preliminary results suggest an important role for detailed observational data coverage for both the description and prediction of regional and continental-scale hydrologic processes over South America.

Tests for numerical irregularities in the rotated, variable resolution approach support the feasibility of the 2-way nest method for present time scales

Acknowledgments. This research was supported by NSF grants ATM0106776, ATM0109241 and NOAA/PACS grant NA030AR4310094 to the University of Utah.

References

Anthes, R. A., 1983: Regional models of the atmosphere in middle latitudes. *Mon. Wea. Rev.*, **111**, 1306-1335.

Campetella, C., and C. Vera, 2002: The influence of the Andes mountains on the South American low-level flow. *Geophys. Res. Lett.*, **29**, No. 17, 1826, doi: 10.1029/ 2002 GLO15541.

Coté, J., J.-G. Desmarais, S. Gravel, A. Methot, A. Patoine, M. Roch, and A. Staniforth, 1998b: The Operational CMC-MRB Global Environmental Multiscale (GEM) Model. Part II: results. *Mon. Wea. Rev.*, **126**, 1397-1418.

Errico, R., and D. Baumhefner, 1987: Predictability experiments using a high-resolution limited-area model. *Mon. Wea. Rev.*, **115**, 488-504.

Gandu, A. W., and J. E. Geisler, 1991: A primitive equations model study of the effect of topography on the summer circulation over tropical South America. *J. Atmos. Sci*., **48**, 1822-1836.

Garstang, M., S. Ulanski, S. Greco, J. Scala, R. Swap, D. Fitzjarrald, D. Martin, E. Browell, M. Shipman, V. Connors, R. Harriss, and R. Talbot, 1990: The Amazon Boundary-Layer Experiment: a meteorological perspective. *Bull. Amer. Meteor. Soc*., **71**, 19-32.

Kalnay, E., M. Kanamitsu, R. Kistler, W. Collins, D. Deavan, L. Gandin, M. Iredell, S. Saha, G. White, J. Woollen, Y. Zhu, M. Chelliah, W. Ebisuzaki, W. Higgins, J. Janowiak, K.C. Mo, C. Ropelewski, J. Wang, A. Leetma, R. Reynolds, R. Jenne, and D. Joseph, 1996: The NCEP/NCAR 40-year reanalysis project. *Bull. Amer. Meteor. Soc*., **77**, 437-471.

Kistler, R., E. Kalnay, W. Collins, S. Saha, G. White, J. Woollen, M. Chelliah, W. Ebisuzaki, M. Kanamitsu, V. Kousky, H. Dool, R. Jenne, and M. Fiorino, 2001: The NCEP-NCAR 50-year reanalysis: monthly means cd-rom and documentation. *Bull. Amer. Meteor. Soc.*, **82**, 247-268.

Kleeman, R., 1989: A modeling study of the effect of the Andes on the summertime circulation over tropical South America. *J. Atmos Sci.*, **46**, 3344-3362.

Langland, R. H., Z. Toth, R. Gelaro, I. Szunyogh, M. A. Shapiro, S. J. Majumdar, R. E. Morss, G. D. Rohaly, C. Velden, N. Bond, and C. H. Bishop, 1999: The North Pacific Experiment (NORPEX-98): targeted observations for improved North American weather forecasts. *Bull. Amer. Meteor. Soc.*, **80**, 1363-1384.

Miguez-Macho, and J. Paegle, 2001: Sensitivity of North American numerical weather prediction to initial state uncertainty in selected upstream subdomains. *Mon. Wea. Rev.*, **129**, 2005-2022.

Nicolini, M., Y. G. Skabar, A. G. Ulke, and A. C. Saulo, 2002: RAMS model performance in simulating precipitation during strong poleward low level jet events

over northeastern Argentina. *Meteorologica*, **27**, 89-98.

Paegle, J., 1989: A variable resolution global model based upon Fourier and finite element representation, *Mon. Wea. Rev*., *117*, 583-606, 1989.

____, Q. Yang, and M. Wang, 1997: Predictability in limited area and global models. *Meteor. Atmos. Phys*., **63**, 53-69.

Ralph, M., and Coauthors, 1999: The California Land-Falling Jets Experiment (CALJET) objectives and design of a coastal atmosphere ocean observing system deployed during a strong El Niño. Preprints, *Third Symp. on Integrated Observing Systems*, Dallas, TX, Amer. Meteor. Soc., 78-81.

Roman, J. C., G. Miguéz-Macho, L. A. Byerle, and J. Paegle, 2004: Intercomparison of global research and operational forecasts, *Wea. Forecasting, in press.*

Saulo, A. C., M. Seluchi, C. Campetella, and L. Ferreira, 2001: Error evaluation of NCEP and LAHM Regional Model daily forecasts over southern South America. *Wea. Forecasting*, **16**, 697-712.

Schultz, D. M., W. J. Steenburgh, R. J. Trapp, J. Horel, D. E. Kingsmill, L. B. Dunn, W. D. Rust, L. Cheng, A. Bansemer, J. Cox, J. Daugherty, D. P. Jorgensen, J. Meitin, L. Showell, B. F. Smull, K. Tarp, and M. Trainor, 2002: Understanding Utah winter storms: the Intermountain Precipitation Experiment. *Bull. Amer. Meteor. Soc*., **83**, 189-21.

Stoelinga, M. T., P. V. Hobbs, C. F. Mass, J. D. Locatelli, B. A. Colle, R. A. Houze, Jr., A. L. Rangno, N. A. Bond, B. F. Smull, R. M. Rasmussen, G. Thompson, and B. R. Colman, 2003: Improvement of microphysical parametrization through observational verification experiment. *Bull. Amer. Meteor. Soc*., **84**, 1807-1826.

White, B. G., J. Paegle, W. J. Steenburgh, J. D. Horel, R. T. Swanson, L. K. Cook, D. J. Onton, and J. G. Miles, 1999: Short-term forecast validation of six models, *Wea. Forecasting*, **14**, 84-108.

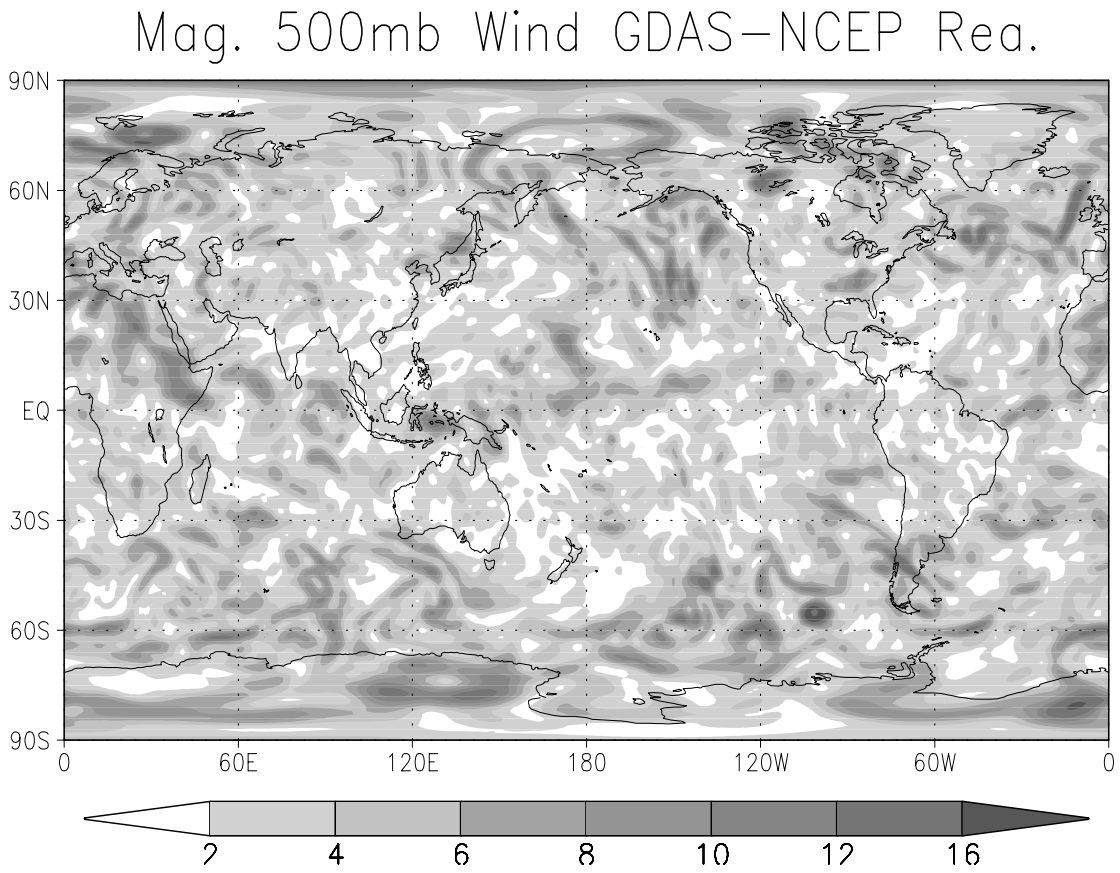

FIG. 1. The magnitude of the differences in 500 mb wind (m/s) between the GDAS analysis and NCEP/NCAR Reanalysis (GDAS minus NCEP/NCAR Reanalysis) at 00 UTC on 17 January 2003. The Reanalysis has been interpolated to 1˚ spacing to match the horizontal resolution of the GDAS analysis.

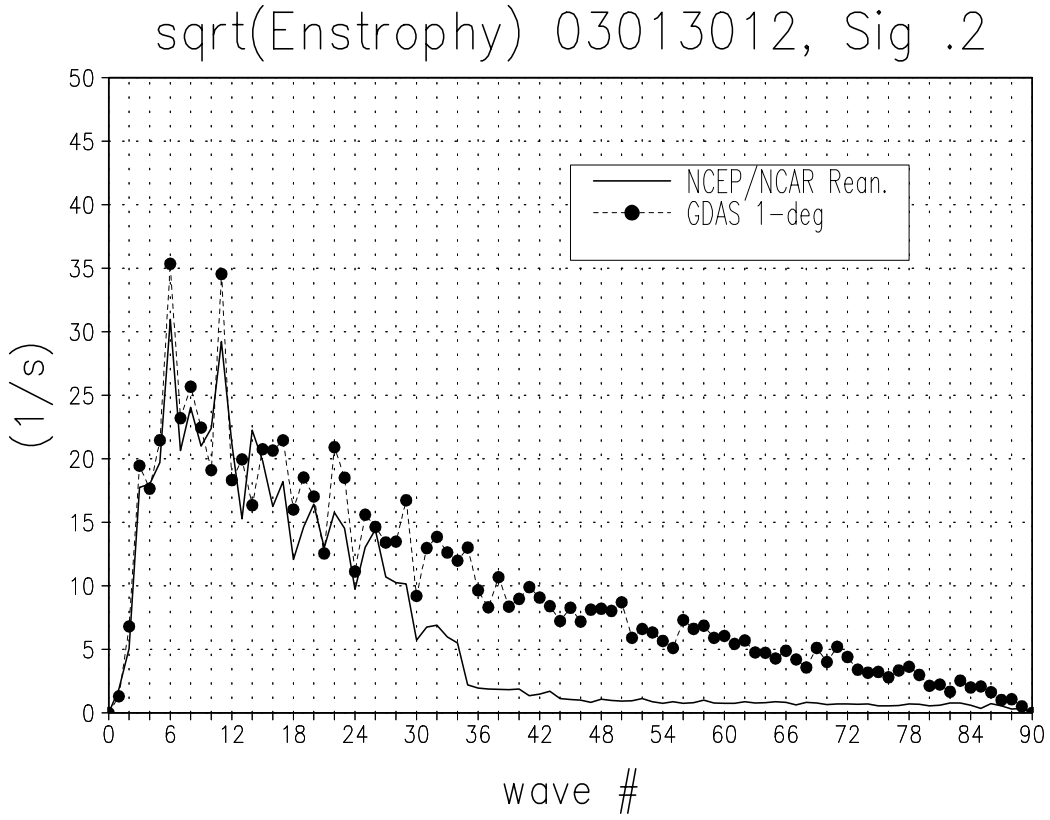

FIG. 2. The square root of the globally averaged enstrophy spectrum (1/s) as a function of wave number at 12 UTC on 30 January 2003, for the NCEP/NCAR Reanalysis (line) and GDAS analysis (circles), at sigma level 0.2.

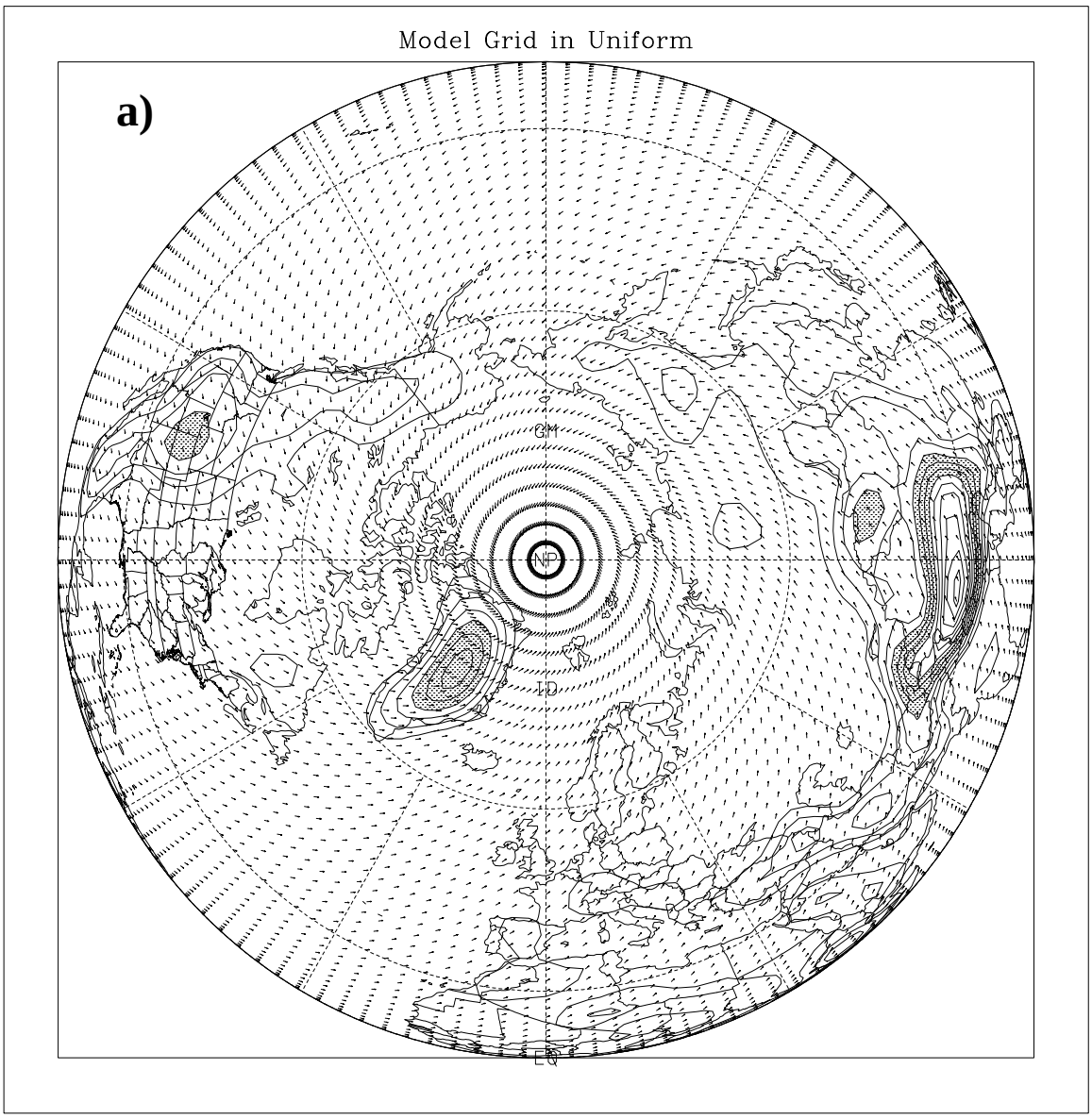

FIG. 3. Utah Global Model grid. (a) Contours of topography with uniform resolution, 129 points in longitude, 91 points in latitude. (b) Similar to (a), but the mathematical pole has been rotated to 10˚S, 60˚W, with the same number of grid points. Latitude spacing is 1˚, north of 45˚N and 3˚ resolution south of 45˚N with respect to the rotated pole. Contours are every 500 m in (a) and (b). Topography higher than 2000 m is shaded in (a).

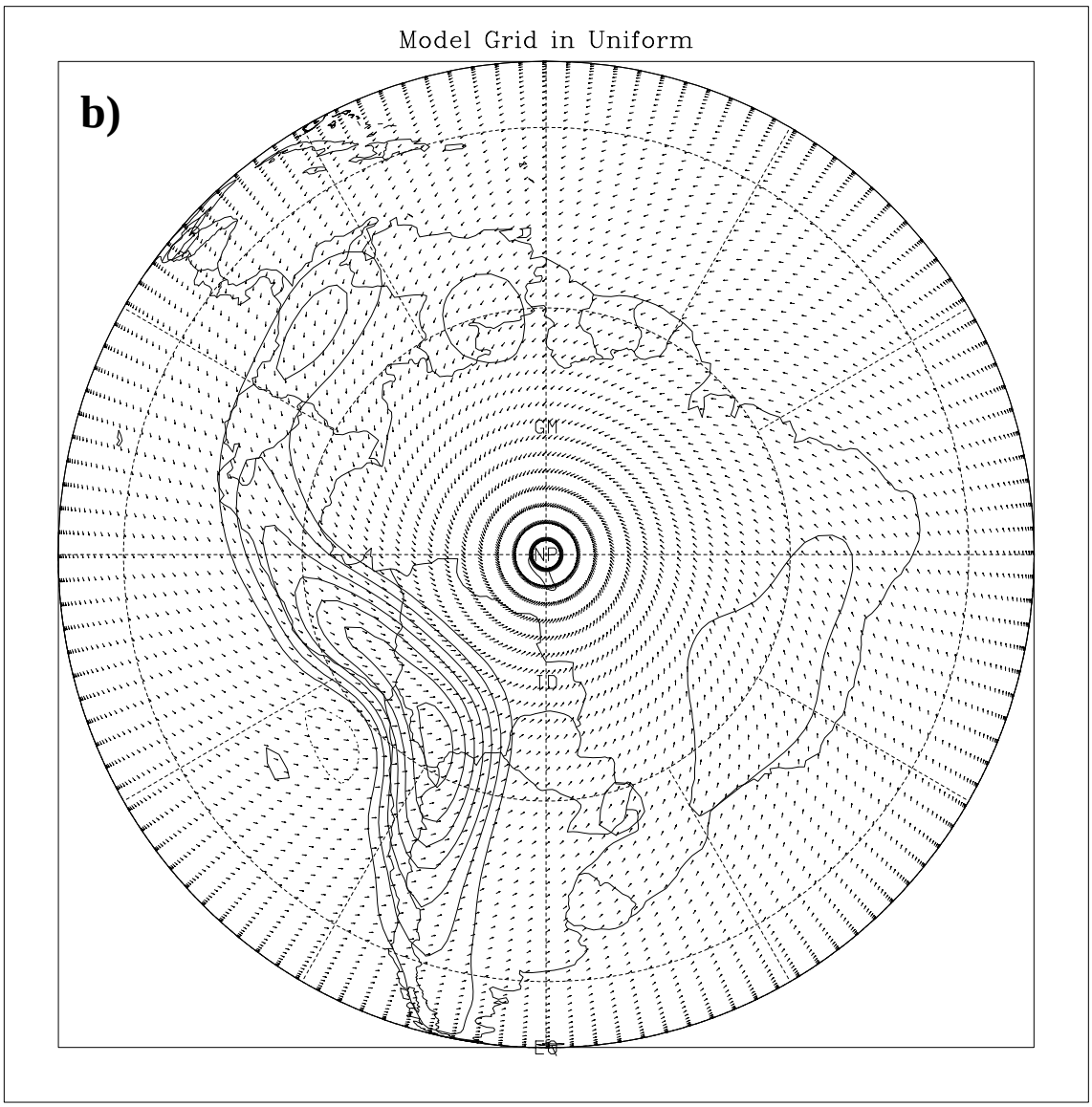

Fig. 3.3, continued.

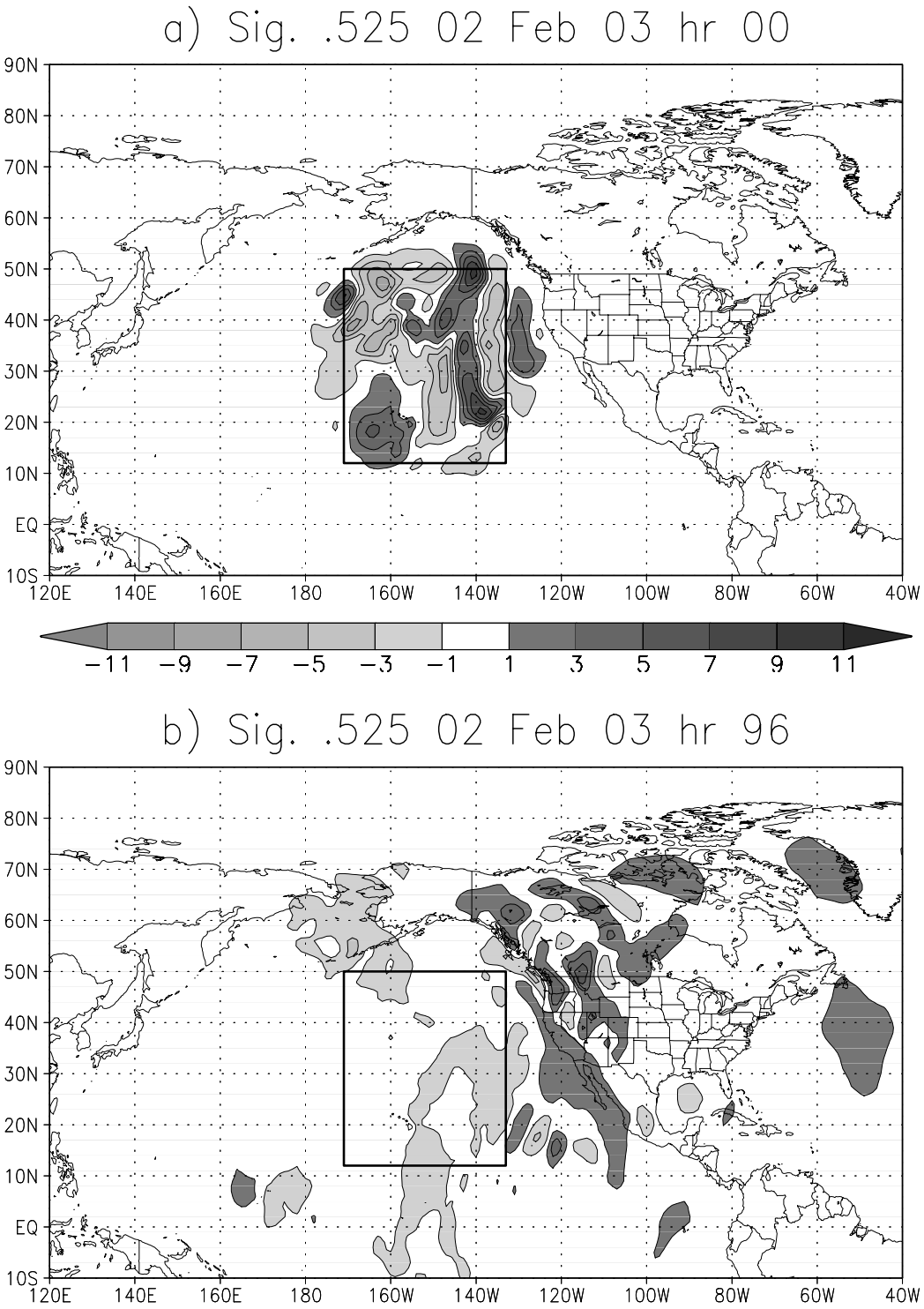

FIG. 4. Meridional flow differences at sigma 0.525 between the experiment with initial uncertainty (NCEP Reanalysis minus GDAS) over the northeast Pacific and the control, intialized with the NCEP Reanalysis globally. (a) Initial time, and (b) forecast hour 96. Units are m/s and the contour interval is 2 m/s. The sign of values is indicated with shading. The validation domain is outlined.

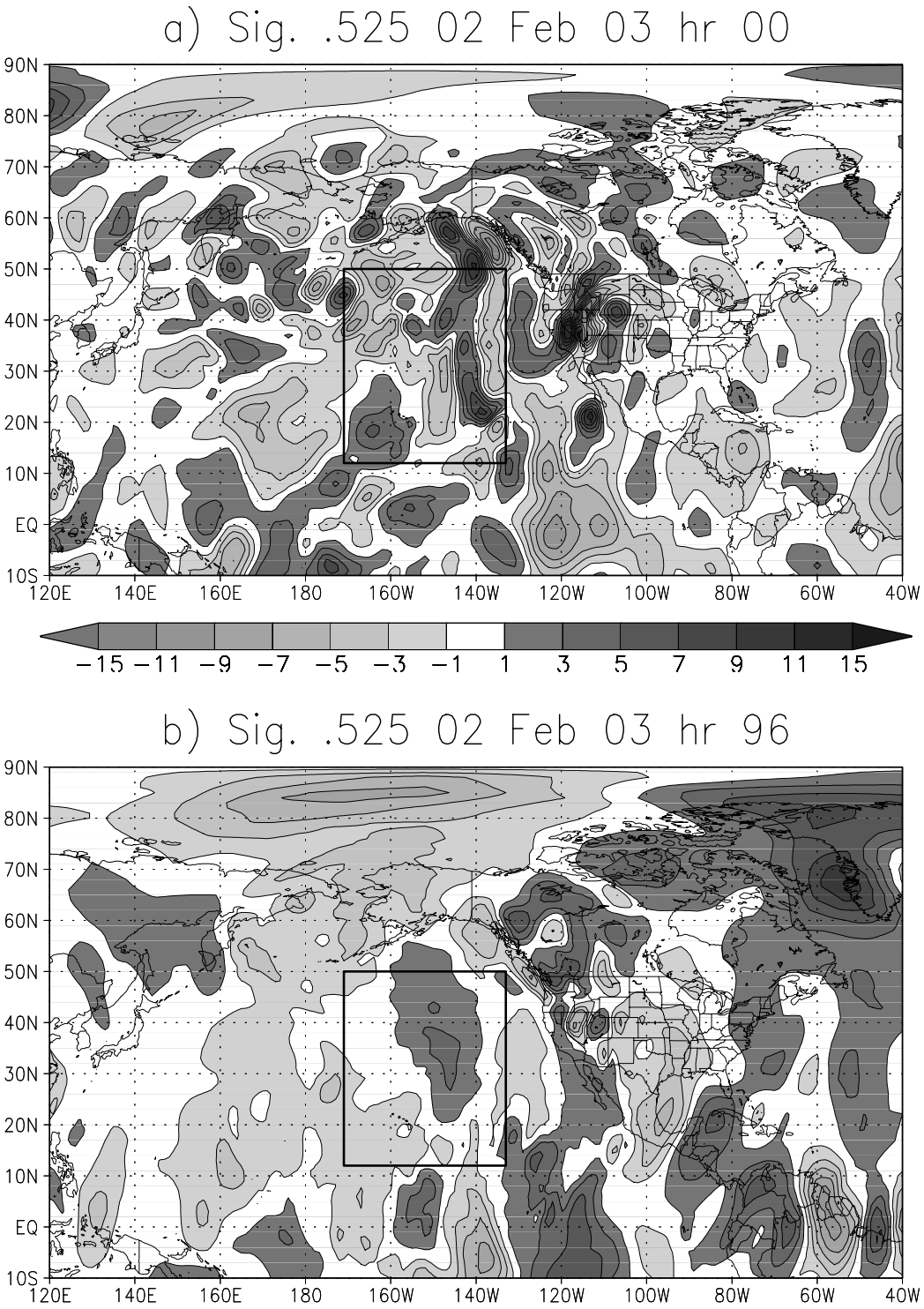

FIG. 5. Meridional flow differences at sigma 0.525 between the experiment with initial uncertainty (NCEP Reanalysis minus GDAS) over the whole globe and the control, intialized with the NCEP Reanalysis globally. (a) Initial time, and (b) forecast hour 96. Units are m/s and the contour interval is 2 m/s. The sign of values is indicated with shading. The validation domain is outlined.

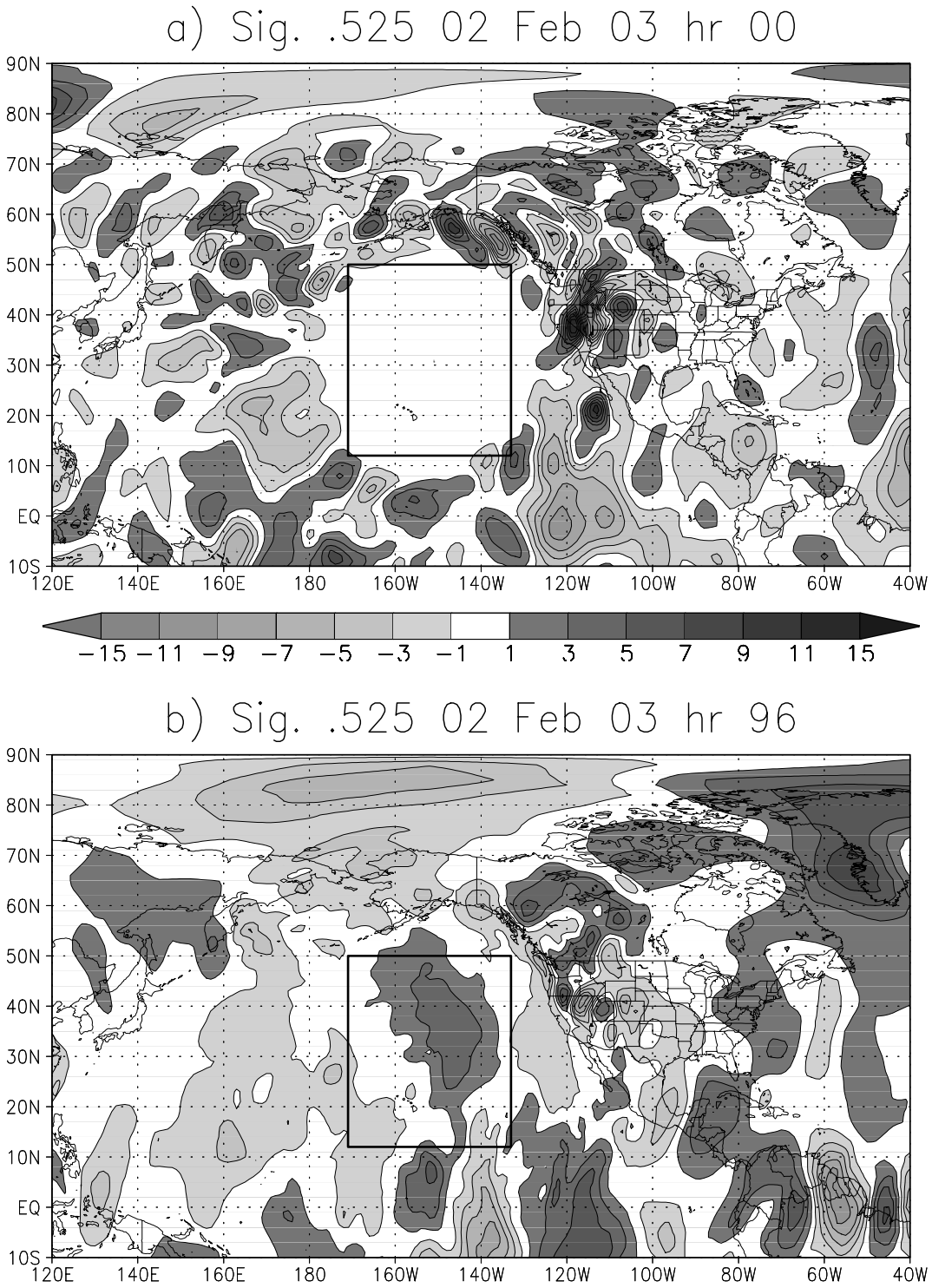

FIG. 6. Meridional flow differences at sigma 0.525 between the experiment with initial uncertainty (NCEP Reanalysis minus GDAS) outside the northeast Pacific and the control, intialized with the NCEP Reanalysis globally. (a) Initial time, and (b) forecast hour 96. Units are m/s and the contour interval is 2 m/s. The sign of values is indicated with shading. The validation domain is outlined.

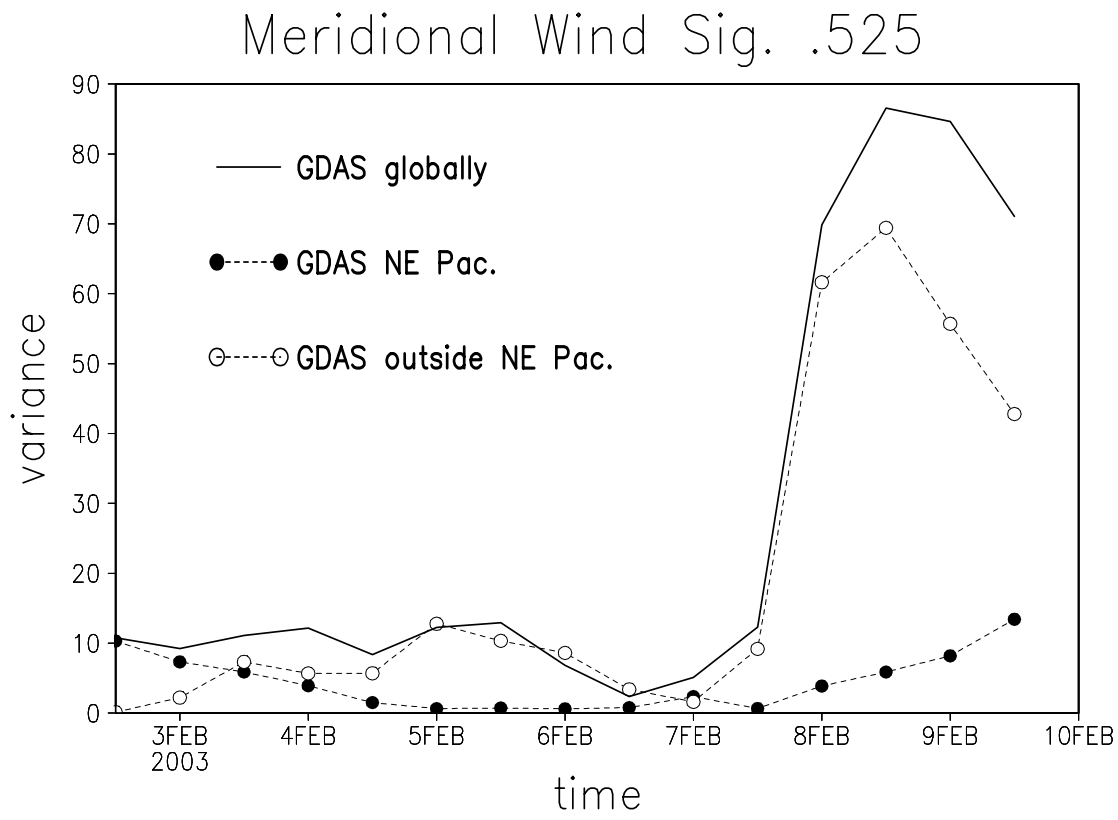

FIG. 7. Variance of the meridional wind at sigma 0.525 computed over the northeast Pacific domain. The solid curve shows the variance with respect to the control (initialized with the NCEP/NCAR Reanalysis, globally) for the experiment initialized globally with the GDAS analysis. Dotted curves are for the experiment with initial uncertainty over the northeast Pacific region (closed circles), and the complementary case, perturbing the rest of the globe (open circles). Units are (m*m)/(s*s).

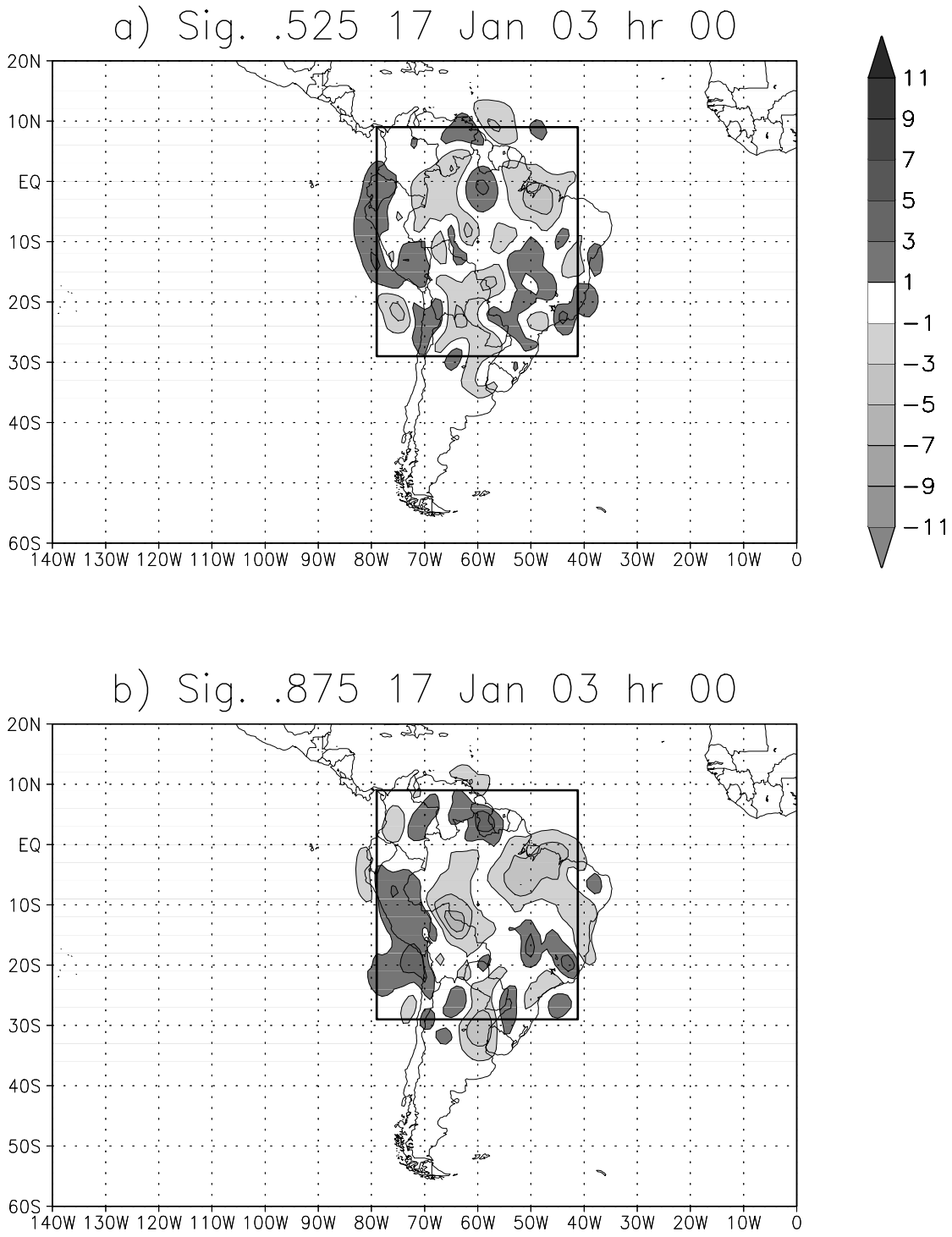

FIG. 8. Meridional flow differences between the experiment with initial uncertainty (NCEP Reanalysis minus GDAS) over South America and the control, intialized with the NCEP Reanalysis globally. (a) Initial time, sigma 0.525; (b) initial time, sigma 0.875; (c) forecast hour 96, sigma 0.525 and (d) forecast hour 96, sigma 0.875. Units are m/s and the contour interval is 2 m/s. The sign of values is indicated with shading. The validation domain is outlined.

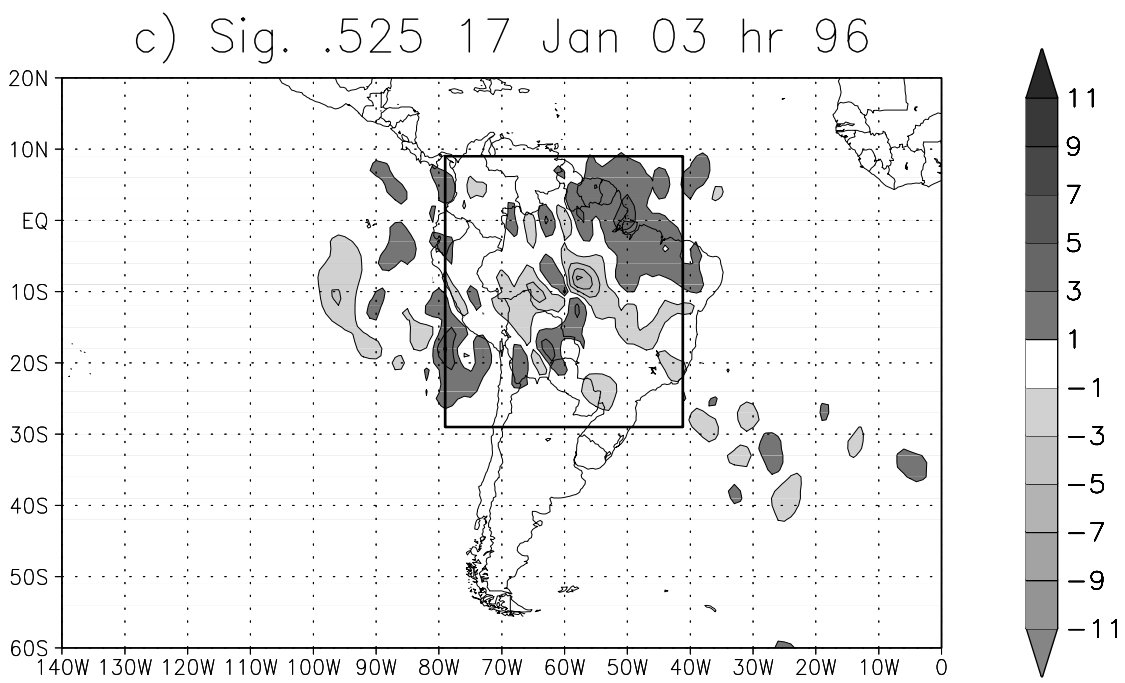

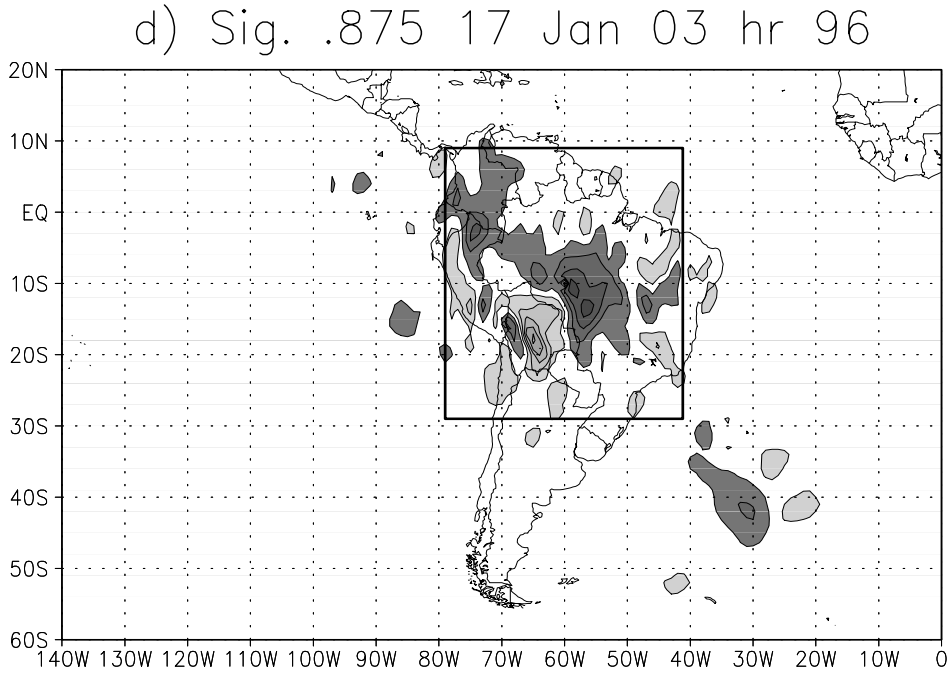

Fig. 3.8, continued.

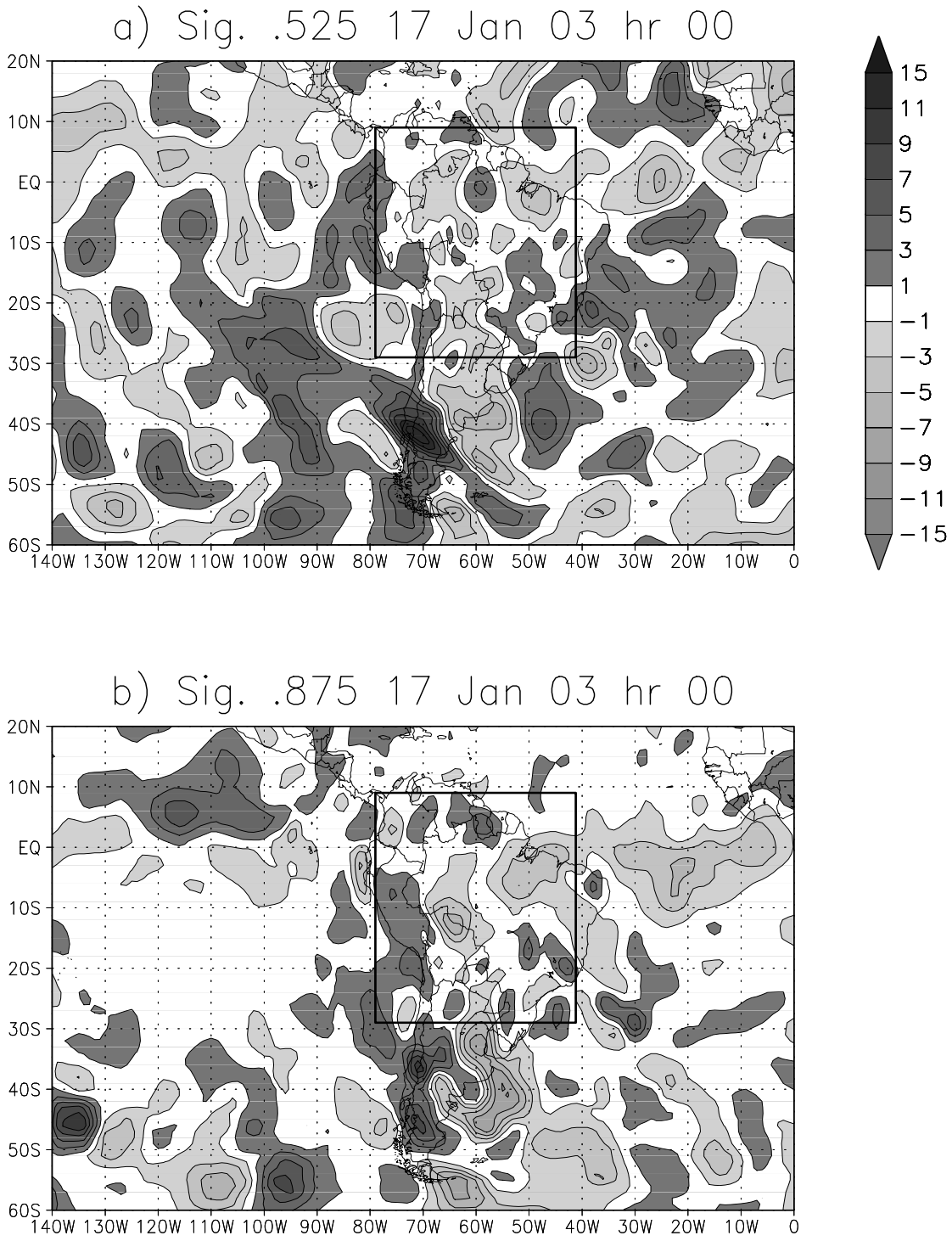

FIG. 9. Meridional flow differences between the experiment with initial uncertainty (NCEP Reanalysis minus GDAS) over the whole globe and the control, intialized with the NCEP Reanalysis globally. (a) Initial time, sigma 0.525; (b) initial time, sigma 0.875; (c) forecast hour 96, sigma 0.525 and (d) forecast hour 96, sigma 0.875. Units are m/s and the contour interval is 2 m/s. The sign of values is indicated with shading. The validation domain is outlined.

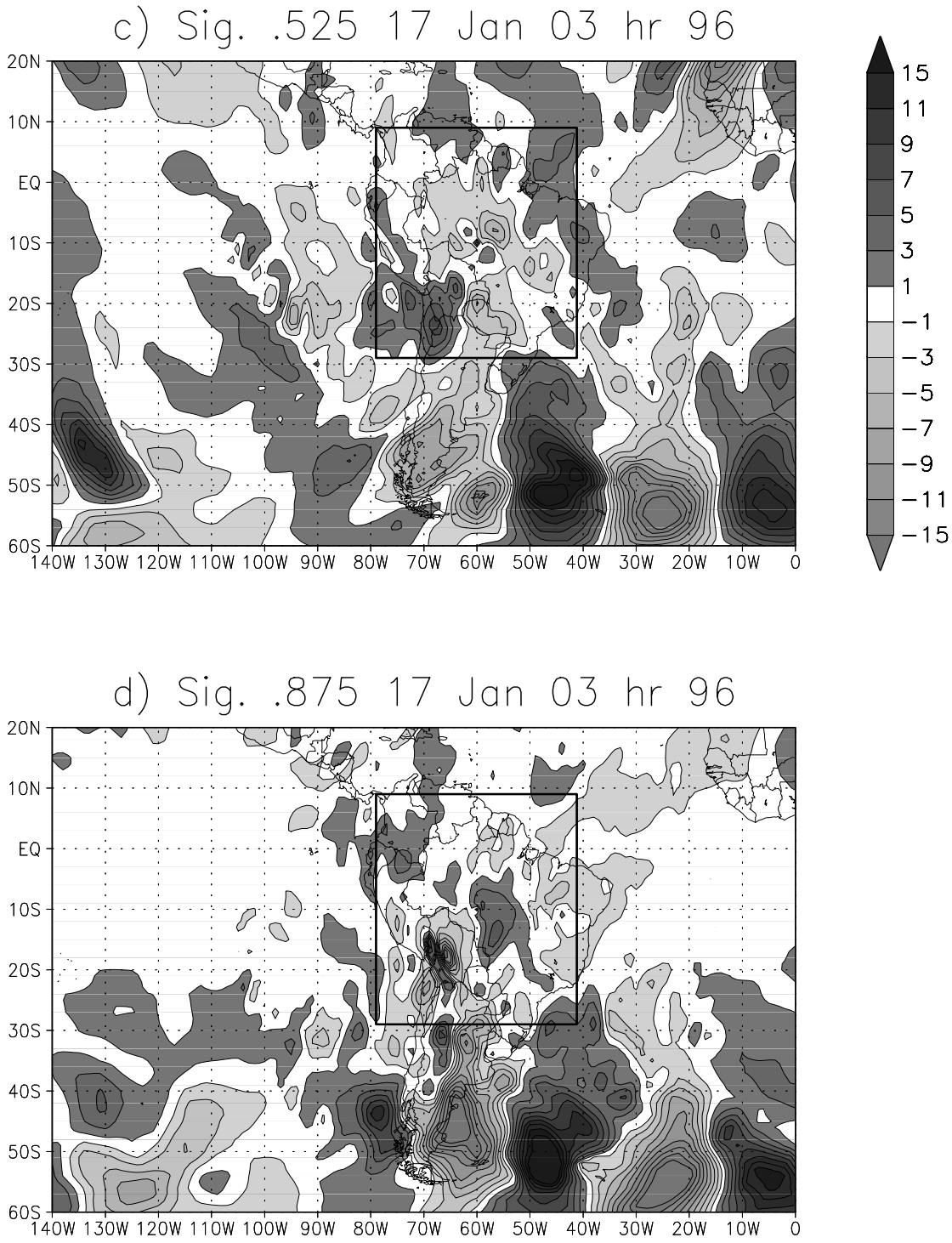

Fig. 3.9, continued.

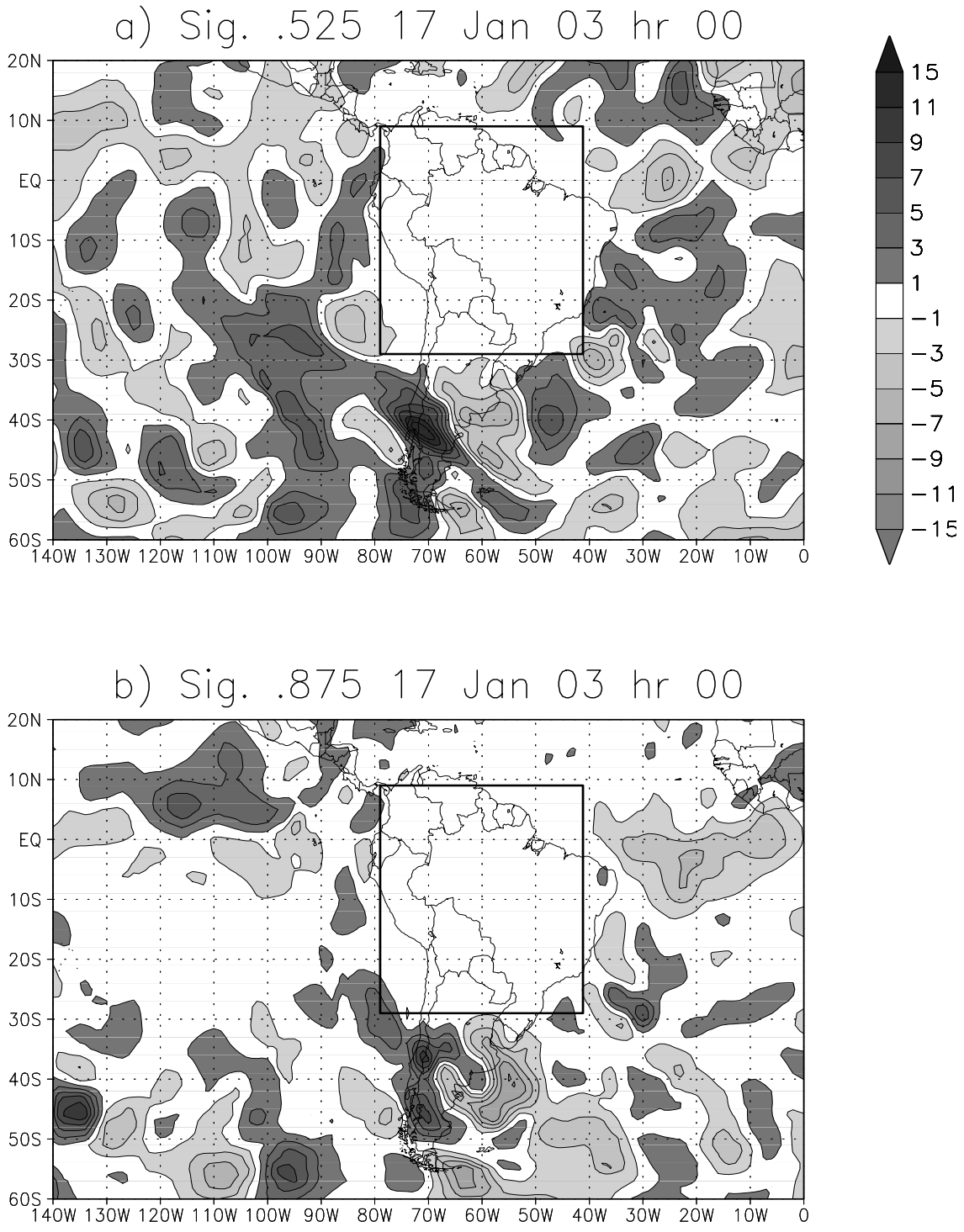

FIG. 10. Meridional flow differences between the experiment with initial uncertainty (NCEP Reanalysis minus GDAS) outside of South America and the control, intialized with the NCEP Reanalysis globally. (a) Initial time, sigma 0.525; (b) initial time, sigma 0.875; (c) forecast hour 96, sigma 0.525 and (d) forecast hour 96, sigma 0.875. Units are m/s and the contour interval is 2 m/s. The sign of values is indicated with shading. The validation domain is outlined.

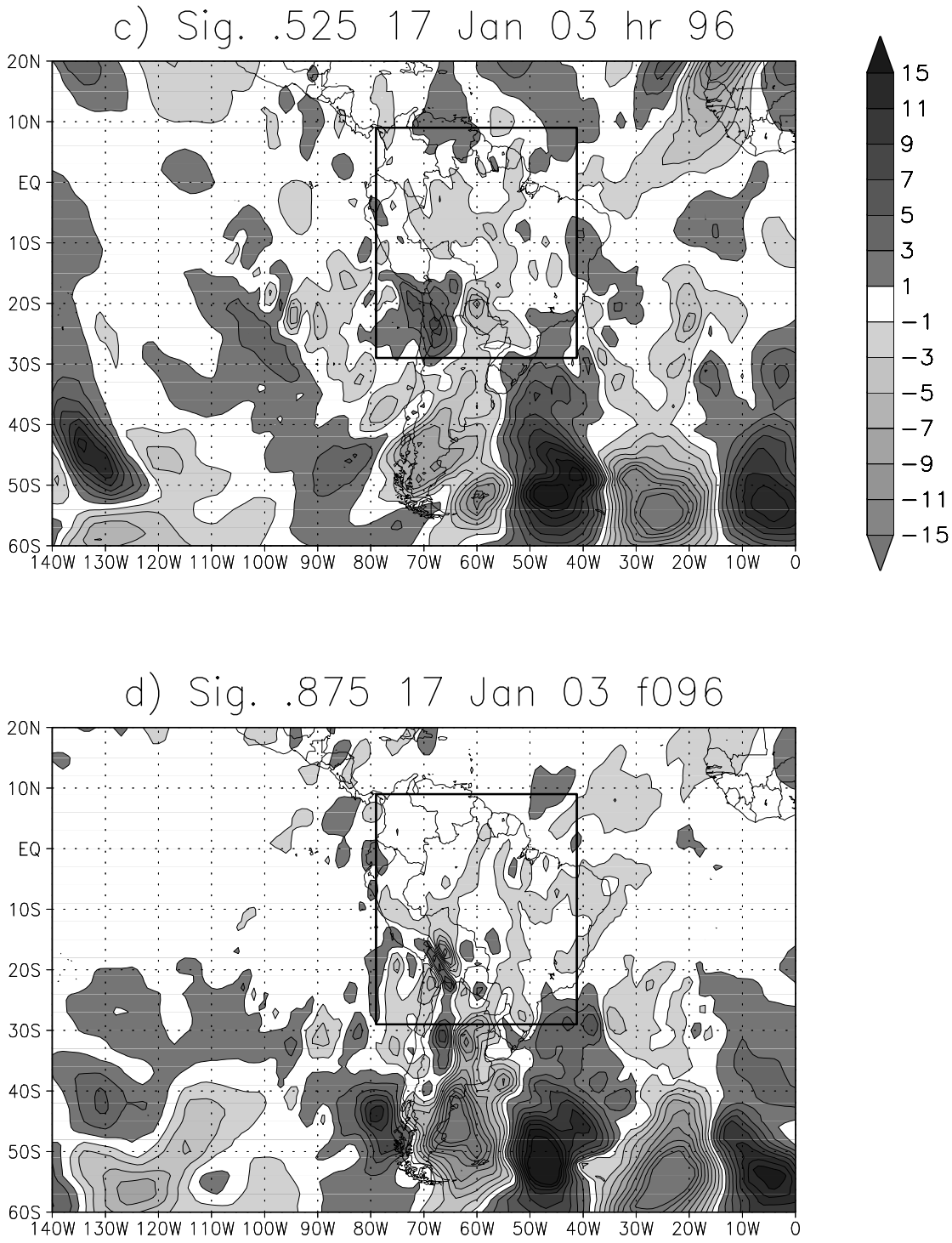

Fig. 3.10, continued.

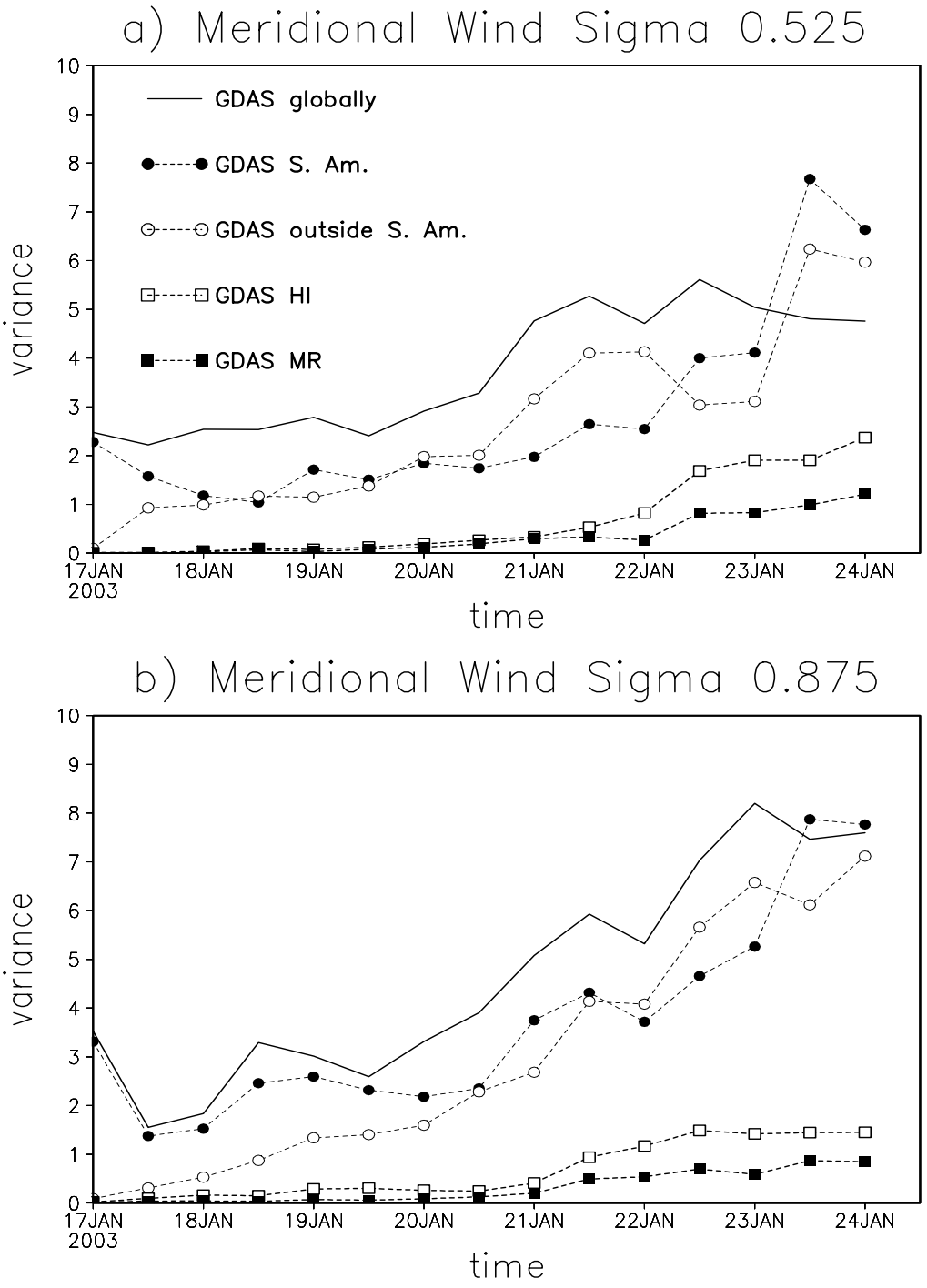

FIG. 11. Variance computed over the South American domain. (a) Meridional wind at (a) sigma 0.525, and (b) sigma 0.875, and (c) specific humidity at sigma 0.875. The solid curve shows variance for the experiment initialized globally from the GDAS analysis. Dashed curves with circles are for the experiment with initial uncertainty over the South American region (closed) and the complementary case, perturbing the rest of the globe (open). Curves with boxes are for the experiments which test numerical sensitivity, described in the text. Units are (m*m)/(s*s) in (a) and (b) and (g*g)/(kg*kg) in (c).

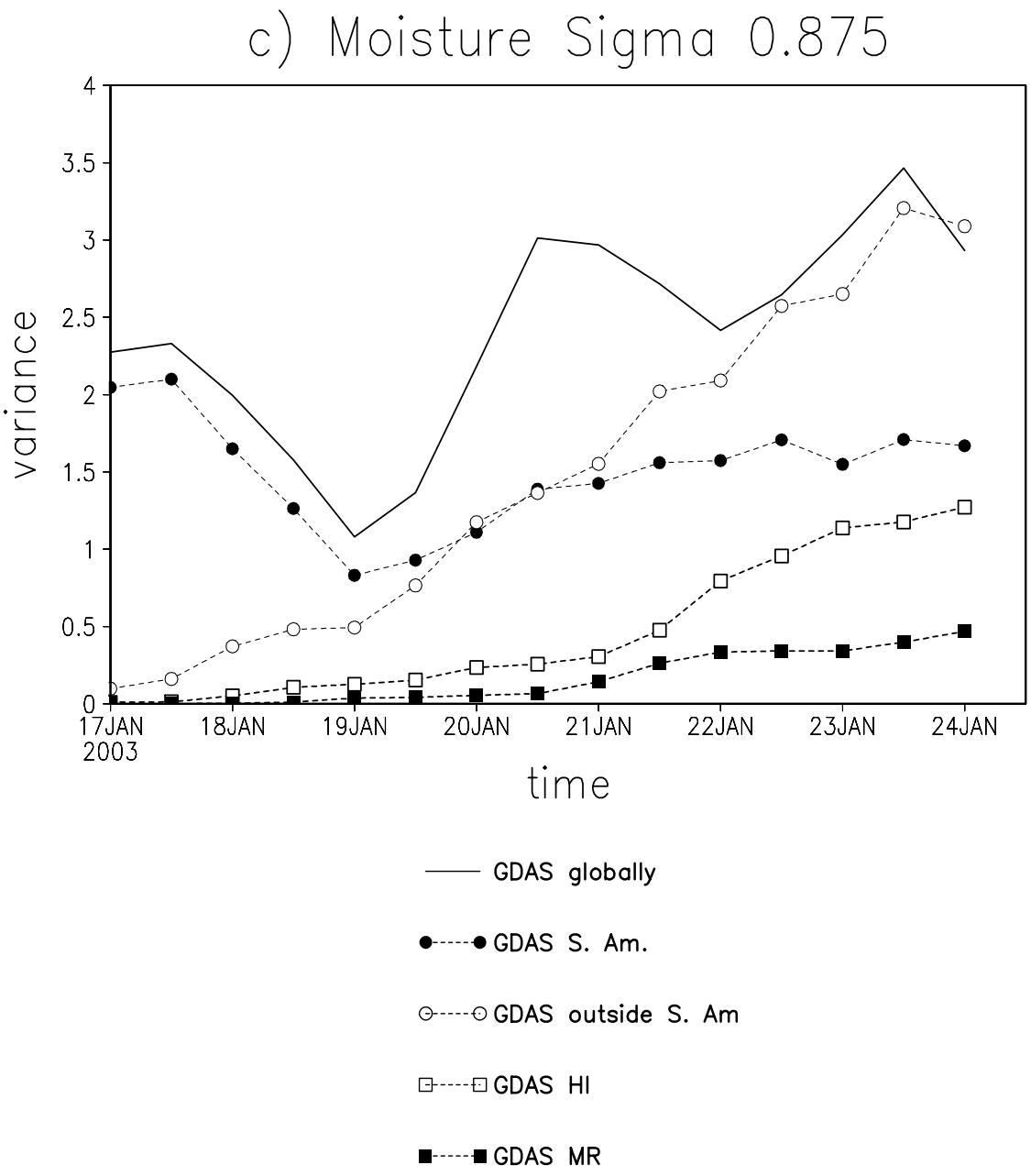

Fig. 3.11, continued.